PHYSICS OF FLUIDS **25**, 063302 (2013)

Wall forces on a sphere in a rotating liquid-filled cylinder

Yoshiyuki Tagawa,[1,2,a)] Jarich van der Molen,[1] Leen van Wijngaarden,[1] and Chao Sun[1,b)]
[1]*Physics of Fluids Group, Faculty of Science and Technology, J. M. Burgers Centre for Fluid Dynamics, University of Twente, PO Box 217, 7500 AE Enschede, The Netherlands*
[2]*Department of Mechanical Systems Engineering, Tokyo University of Agriculture and Technology, Koganei Campus 6-507, 2-24-16 Nakacho, Koganei-city, Tokyo, Japan*

(Received 4 September 2012; accepted 23 May 2013; published online 24 June 2013)

We experimentally study the behavior of a particle slightly denser than the surrounding liquid in solid body rotating flow. Earlier work revealed that a heavy particle has an unstable equilibrium point in unbounded rotating flows [G. O. Roberts, D. M Kornfeld, and W. W Fowlis, J. Fluid Mech. **229**, 555–567 (1991)]. In the confinement of the rotational flow by a cylindrical wall a heavy sphere with density 1.05 g/cm^3 describes an orbital motion in our experiments. This is due to the effect of the wall near the sphere, i.e., a repulsive force (F_W). We model F_W on the sphere as a function of the distance from the wall (L): $F_W \propto L^{-4}$ as proposed by Takemura *et al.* [J. Fluid Mech. **495**, 235–253 (2003)]. Remarkably, the path evaluated from the model including F_W reproduces the experimentally measured trajectory. In addition during an orbital motion the particle does not spin around its axis, and we provide a possible explanation for this phenomenon. © *2013 AIP Publishing LLC*. [http://dx.doi.org/10.1063/1.4811406]

I. INTRODUCTION

Forces acting on a sphere in various flows are of importance from a fundamental point of view and in applications (see the review article[1]). A natural approach for analyzing the forces in complex flows is to decouple the flow effect into those of typical flows, like a solid-body rotating flow. In recent years the forces on particles lighter than the surrounding fluid were studied in a solid body rotating flow around a horizontal axis (i.e., gravity is perpendicular to the rotation axis) in Refs. 2–7. The advantage of this system is that buoyant particles reach an equilibrium point, from which drag and lift coefficients are well determined over a wide range of dimensionless parameters. Provided the equilibrium point is sufficiently far from the wall(s) bounding the rotating flow, this can be considered as unbounded. In this way drag and lift forces as well as particle spin have been measured at moderate Reynolds numbers and reported in the above mentioned papers. A particle heavier than surrounding liquid spirals outward in rotating flow, i.e., it has an unstable equilibrium point. Such orbits were calculated by Roberts *et al.*[8] for such small particles that Stokes flow can be assumed. They also took no lift forces into account.

The effect of the wall is important but less intensively studied, especially at moderate-to-high Reynolds numbers. It has been investigated mainly in the situation of a sphere moving parallel to a flat plate or rotating near a plane boundary. The influence of a vertical flat wall on a spherical rising bubble is studied experimentally by Takemura *et al.*[9] and numerically by Zeng *et al.*[10] for Reynolds number less than 100. Takemura *et al.*[9] discussed two hydrodynamical mechanisms of wall interaction, one due to the vorticity generated at the bubble surface and the other due to the irrotational dipole associated with the bubble motion. They proposed empirical correlations based on

a)Electronic mail: tagawayo@cc.tuat.ac.jp
b)Electronic mail: c.sun@utwente.nl

the strength of these two mechanisms, leading to practical expressions of the lift force as a function of Reynolds number and the distance between the wall and the particle. Liu *et al.*[11] studied the effect of the spin of the sphere in the presence of no-slip planar boundaries. They found that for small sphere-wall gap widths and Reynolds numbers ∼1 viscous effect plays a role causing repulsive forces while larger Reynolds numbers ∼100 cause a Bernoulli effect in the gap, which may turn the forces into attractive ones.

When it comes to rotating flow, the wall effect is studied for very viscous flow. Ashmore *et al.*[12] investigated the interaction of the wall with a dense steel particle in the Stokes flow regime. Mullin *et al.*[13] found that with a very heavy sphere in a highly viscous rotating fluid three regimes can be distinguished as a function of the cylinder rotating speed, which we will discuss in Sec. IV.

In this paper we experimentally investigate the trajectories of particles, slightly heavier than the rotating fluid in which the particles are introduced. In particular we are interested in the interaction of the particle with the cylinder wall for high Reynolds numbers $O(10^3)$. The translational and rotational motion of the spheres are observed with the help of Particle Tracking Velocimetry (PTV) and orientation detection software,[14] respectively. In addition, we use Particle Image Velocimetry (PIV) to record the velocity distribution in the undisturbed as well as in the disturbed fluid.

The outline of this paper is as follows. In Sec. II the equation of motion of a particle is introduced. The experimental setup is described in Sec. III. The results are shown in Sec. IV, followed by concluding remarks in Sec. V.

II. FORCES ACTING ON A PARTICLE

The force balance on a sphere in the present condition is

$$\rho_p V_p \frac{d\boldsymbol{u}}{dt} = \boldsymbol{F_A} + \boldsymbol{F_L} + \boldsymbol{F_D} + \boldsymbol{F_G} + \boldsymbol{F_I} + \boldsymbol{F_W}, \tag{1}$$

where ρ_p is the density of the particle, V_p the volume of the particle, $\boldsymbol{u}$ the particle velocity, $\boldsymbol{F_A}$ the added mass force, $\boldsymbol{F_L}$ the lift force, $\boldsymbol{F_D}$ the drag force, $\boldsymbol{F_G}$ the gravity force or body force, $\boldsymbol{F_I}$ the force due to acceleration of the flow, and $\boldsymbol{F_W}$ the wall repulsive force. All forces on the particle in the rotating flow are shown in Fig. 1. The operators d/dt and D/Dt are material derivatives going with the particle and with the fluid, respectively. Owing to the fact that the present configuration is quite similar to that of light particles investigated by Bluemink *et al.*,[5] we can adopt expressions for $\boldsymbol{F_A}$, $\boldsymbol{F_L}$, $\boldsymbol{F_D}$, $\boldsymbol{F_G}$, and $\boldsymbol{F_I}$ from Refs. 1 and 15. The full differential equation with all relevant

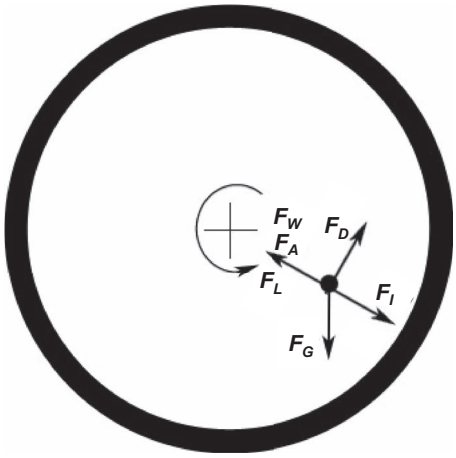

FIG. 1. Forces acting on a particle: $\boldsymbol{F_A}$ the added mass force, $\boldsymbol{F_D}$ the drag force, $\boldsymbol{F_L}$ the lift force, $\boldsymbol{F_G}$ the gravity force or body force, $\boldsymbol{F_I}$ the force due to acceleration of the flow, and $\boldsymbol{F_W}$ the wall repulsive force.

variables is

$$\rho_p V_p \frac{d\boldsymbol{u}}{dt} = \rho V_p C_A \left(\frac{D\boldsymbol{U}}{Dt} - \frac{d\boldsymbol{u}}{dt} \right) + \rho V_p C_L (\boldsymbol{U} - \boldsymbol{u}) \times (\boldsymbol{\nabla} \times \boldsymbol{U}) + \frac{1}{2} \rho A_p C_D |\boldsymbol{U} - \boldsymbol{u}| (\boldsymbol{U} - \boldsymbol{u}) + (\rho_p - \rho) V_p \boldsymbol{g} + \rho V_p \frac{D\boldsymbol{U}}{Dt} + \boldsymbol{F_W}, \quad (2)$$

where ρ is the density of the fluid, C_A the added mass coefficient (C_A=1/2 for the sphere case), $\boldsymbol{U}$ the velocity of the fluid, C_L the lift coefficient normalized with the vorticity $\boldsymbol{\nabla} \times \boldsymbol{U}$, A_p the cross sectional area of the sphere, C_D the drag coefficient, and $\boldsymbol{g}$ the acceleration of gravity.

We have not found results on the magnitude of a wall induced force $\boldsymbol{F_W}$ in the case of a curved wall, as is ours. Since the radius of the sphere is small with respect to the drum radius, we may confidently use the results for a flat wall. Recent work, relevant for our case, is given by Takemura *et al.*[9] and Zeng *et al.*[10] From these works it is clear that there are two mechanisms which contribute to $\boldsymbol{F_W}$. The first is the vorticity distribution in the wake behind the sphere. This diffuses outward, but this process is asymmetric due to the presence of the wall. It leads to a wall force away from the wall. On the other hand the accelerated flow through the gap between the sphere and the wall produces an attractive force. The first mechanism is dominant over a wide range of Reynolds numbers. Takemura *et al.*[9] did experiments at Reynolds number of order 10^2 and over a large range of the ratio between distance from a wall L and sphere radius R, i.e., L/R. They summarized their results as follows:

$$F_W = C_W A_p \rho u^2/2, \quad (3a)$$

where

$$C_W = C_{W0}(L^*) a^2(Re)(L/\gamma R)^{g(Re)} \quad (3b)$$

with

$$\gamma \approx 3.0, \quad g(Re) \approx -2.0 \tanh(0.01Re), \quad a(Re) \approx 1 + 0.6Re^{1/2} - 0.55Re^{0.08} \quad \text{for } 1 \le Re \le 100, \quad (3c)$$

$$C_{W0}(L^*) = \begin{cases} (9/8 + 5.78{*}10^{-6} L^{*4.58}) \beta^2 \exp(-0.292 L^*) & \text{for } 0 < L^* < 10 \\ 8.94 \beta^2 L^{*-2.09} & \text{for } 10 \le L^* < 300, \end{cases} \quad (3d)$$

where $\beta = 1$ for a rigid sphere, the dimensionless separation $L^* = LU/\nu$, the Reynolds number $Re = Ud_p/\nu$, based on the particle diameter d_p and the oncoming fluid velocity at the particle location U.

Zeng *et al.*[10] performed numerical calculations for the situation of the experiments by Takemura *et al.*,[9] and found a good agreement with Eqs. (3a)–(3d) in the relevant parameter range. Although our Reynolds numbers are larger than those in the experiments of Takemura *et al.*,[9] we assume that the relations expressed by Eqs. (3a)–(3d) still hold.

We choose cylindrical coordinates (r, ϕ, z) with z along the rotation axis. Since during the experiments, to be described in Sec. III, the particle always stays in a plane perpendicular to the rotation axis, the momentary position is sufficiently described by $\boldsymbol{r} = \boldsymbol{r}(r, \phi)$. With a constant angular velocity ω, the flow velocity is

$$\boldsymbol{U}(\boldsymbol{r}) = \omega r \boldsymbol{e_\phi}, \quad (4)$$

where $\boldsymbol{e}_\phi$ is the unit vector in azimuthal direction. In terms of this coordinate system, Eq. (2) becomes

$$\ddot{r} = \left(\frac{1}{\rho_p + C_A \rho} \right) \left(\left(\rho_p + C_A \rho \right) r \dot{\phi}^2 + \left(\rho - \rho_p \right) g \sin\phi - \frac{3}{8R} C_D \rho \sqrt{\dot{r}^2 + \left(r \left(\dot{\phi} - \omega \right) \right)^2} \dot{r} + 2 C_L \rho \omega r \left(\omega - \dot{\phi} \right) - \rho r \omega^2 (C_A + 1) + F_W \right) \quad (5a)$$

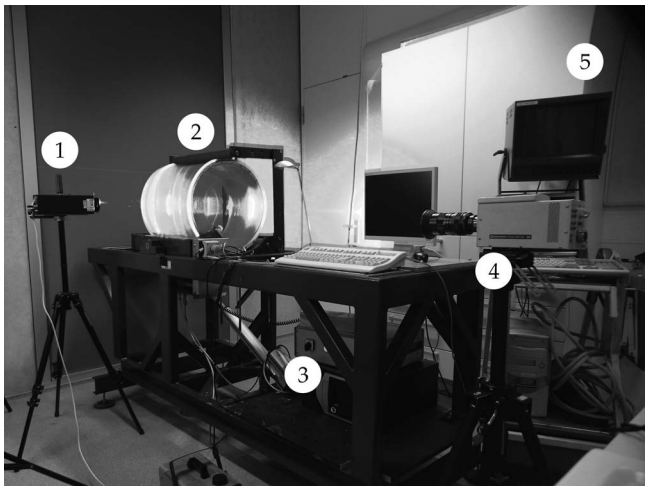

FIG. 2. Experimental setup. 1. Laser, 2. Drum, 3. Drum controller, 4. Camera, 5. Camera controller.

for the radial direction. For the azimuthal direction, we obtain

$$\ddot{\phi} = \left(\frac{1}{r\left(\rho_p + C_A\rho\right)}\right)\left(-2\left(\rho_p + C_A\rho\right)\dot{r}\dot{\phi} + \left(\rho - \rho_p\right)g\cos\phi + \frac{3}{8R}C_D\rho\sqrt{\dot{r}^2 + \left(r\left(\dot{\phi} - \omega\right)\right)^2}r\left(\omega - \dot{\phi}\right) + 2C_L\rho\omega\dot{r}\right). \tag{5b}$$

The dots denote differentiation with respect to time.

III. EXPERIMENTAL SETUP

Figure 2 shows the experimental setup. The cylindrical acrylic drum is 500 mm long and has an outer radius of 250 mm with 15 mm thick plastic walls and lids. Its axisymmetric axis is horizontal. Two steel rods with rubber coatings support it and one of them rotates driven by an AC servo motor. We vary the frequency of the drum f_d in the range of 0–2 Hz. The drum is filled with de-ionized water with density 1.00 g/cm^3. We use polystyrene spheres with density 1.05 g/cm^3, slightly heavier than the fluid. Their size ranges from 10 to 60 $\pm$ 0.01 mm. The adsorption of de-ionized water by polystyrene is less than one percent by volume.

Particle trajectories are recorded by using a high-speed camera (Kodak 2000, Redlake Co., USA/Photron SA.1, Photron Co., Japan) with a lens (Fujinon TV Zoom lens). Recording speeds are between 60 frames per second (fps) and 500 fps. In general, the measurement time is about 6 min which corresponds to more than 20 particle trajectory cycles. To ensure stable orbits, the drum is left rotating at constant frequency together with the inserted particle for more than 45 min before starting each measurement. In all the measurements the particle was at the same z-plane position and we have conducted the calibration at the plane through this position. Moreover we open the diaphragm of the lens on the camera so that we have a small depth of focus $\sim$1 cm. This leads to a measurement error within 1 mm.

The recorded images are analyzed with a PTV software. The particle center detected by the use of a circular Hough transform method represents its position. The position of the wall of the drum is determined using particle reflection images. As shown in Fig. 3(a), the lid of the drum has scratched areas at radial position between 15.5 cm and 17 cm. When the particle is located in the scratched area, we determine the particle position using linear interpolation. A rectangular obstacle is located around (0, 0), as shown in Fig. 3(a). We have shown these regions, inaccessible for measurements, in gray color in Fig. 3(b). The error bar in Fig. 3(c) shows the error of our PIV measurements.

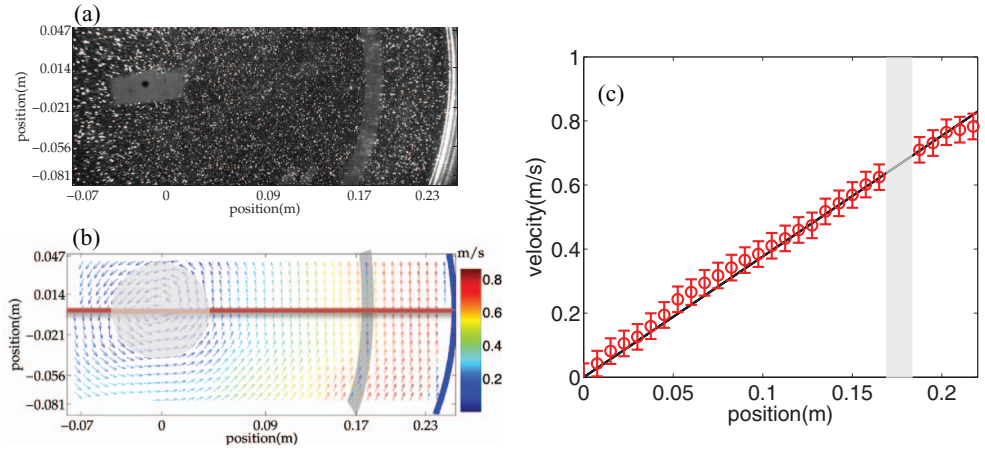

FIG. 3. Solid-body rotational flow at a drum frequency of 0.60 Hz. (a) A snapshot of the PIV tracer particles. (b) Flow field inside the rotating drum. The scratched region is highlighted in gray color. The red line shows the position of the velocities shown in (c). (c) Velocity vs. position along a horizontal line shown in (b). The markers (red online) show the measured velocities and the black line is the theoretical velocity of solid body rotating flow.

The fluid velocity in the drum is measured using PIV technique with a laser sheet (Lasiris Magnum 2, StockerYale on Coherent Inc., Canada). The laser-beam illuminates a cross-sectional area of the drum. The flow field at the drum frequency f_d= 0.60 Hz, without a sphere, is recorded at 1000 fps and an exposure time of 1 μs. Figure 3(b) shows the flow field resulting from averaging over 250 frames. This shows a solid-body rotation. The velocity along the horizontal line (solid red line in Fig. 3(b)) is shown in Fig. 3(c) with the theoretical line of the solid body rotation. The scratched area from 15.5 to 17 cm in radial position is indicated in gray color, where the mean velocity cannot be measured. The experimental result agrees well with the predicted line within error bars, confirming that the flow is a solid body rotation.

IV. RESULTS AND DISCUSSIONS

We describe what a particle of radius 7 mm, density 1.05 g/cm^3 does when immersed in the rotating flow and the drum frequency f_d is increased from 0 to 1.8 Hz. Much of its behavior is similar to that of heavy particles as described in Ref. 13, mentioned in the introduction. For $f_d < 0.07$ Hz the particle rolls along the drum wall at a fixed position as regarded in the laboratory frame. This is what Mullin *et al.*[13] call the fixed point regime shown as trajectory (1) in Fig. 4. The other regimes mentioned in Ref. 13 are found as well. For 0.11 Hz $\leq f_d <$ 1.2 Hz the particle touches the drum wall in a part of the orbit and falls down in the remainder. This is the cascading regime (trajectory (2) in Fig. 4). For $f_d \geq$ 1.2 Hz the particle sticks on the wall of the drum and rotates with it. This is the fixed solid body regime (trajectory (3) in Fig. 4).

However, we found that our particle, *slightly* heavier than the fluid, floats through the drum, without contacting the drum wall, at drum frequencies between 0.07 and 0.11 Hz. We call this the suspension regime shown as trajectory (4) in Fig. 4. Clearly this is only possible by the presence of the wall. In the remaining part of this section we focus on the particle motion in this regime.

The positions of the particle are plotted in Fig. 5 for several drum frequencies f_d. The coordinates of the particle positions in Fig. 5 are made dimensionless with the help of the particle radius. The trajectories show almost perfect circles. The minimum dimensionless distance to the wall is $\sim$1 for all cases. Equilibrium points of the dynamical system described by Eqs. (5a) and (5b) are found by requiring $\ddot{r} = \dot{r} = \ddot{\phi} = \dot{\phi} = 0$. Inserting this into Eq. (5) gives the relations

$$C_D = \frac{4}{3}\frac{gd(\rho_p - \rho)\cos\phi_e}{\rho r_e^2 \omega^2}, \tag{6a}$$

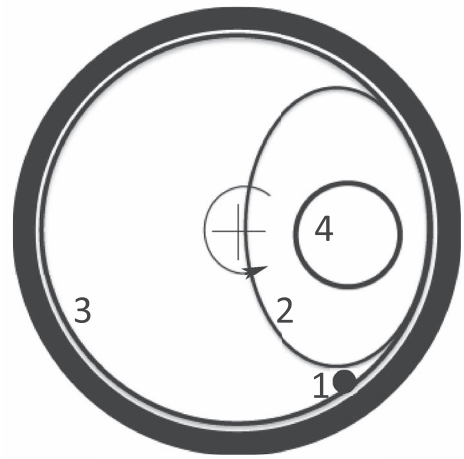

FIG. 4. Four regimes of a heavy particle trajectory: (1) Fixed-point regime, (2) cascading regime, (3) fixed solid body rotation regime, and (4) suspension regime.

$$C_L = \frac{1}{2}(1 + C_A - \frac{(\rho_p - \rho)g \sin\phi_e}{\rho r_e \omega^2}). \tag{6b}$$

In Fig. 5 we see that the particles do not stay in one point but describe orbits, the radius increasing with f_d, around central positions which are shown as cross symbols in Fig. 5 and which we identify with (r_e, ϕ_e) in Eq. (6). Apparently the equilibrium points are not stable in the sense that upon a small displacement the particle returns to the original position. However, it does not spiral outward or inward as in the study of Roberts *et al.* ,[8] but remains in orbit about (r_e, ϕ_e). The explanation for this is that in the analysis of Roberts *et al.*[8] there is no lift force. In our experiments, the range of the position of the center for each cycle includes $y/R = 0$ in Fig. 5. For simplicity for the following discussion, here we approximate ϕ_e as zero. Then the drag is vertical and balances effective gravity. Further the central force exerted by the pressure gradient in the rotating fluid is balanced by the lift

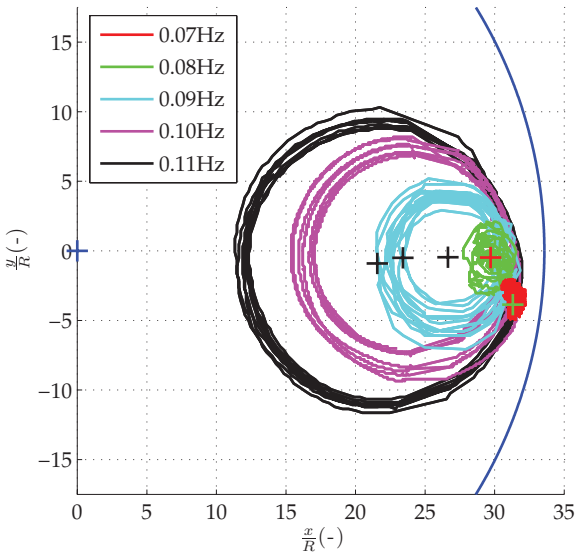

FIG. 5. Particle position of a 7 mm polystyrene particle in a drum for frequency 0.07–0.11 Hz. The cross markers show the average positions for each trajectory.

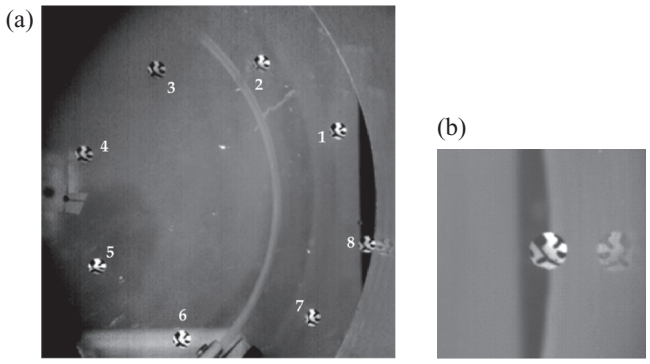

FIG. 6. Images of a particle slightly heavier than the fluid with black and white texture in a drum. (a) Snapshots of a particle in orbital motion. (b) Zoomed image for a particle close to the wall.

force. Hence in $r = r_e$, $\phi = \phi_e = 0$, there is an equilibrium. Now, when the particle undergoes a virtual displacement in r-direction, it meets with a drag which is in excess of the buoyancy force and hence moves upward. Then, it acquires a $\dot{\phi}$, by which the lift is reduced and it is pushed inward by the pressure force. In the case of Roberts *et al.*[8] there is no lift force and so the pressure gradient force is not balanced in $r = r_e$, $\phi = 0$. A picture of an orbit as measured by us is shown in Fig. 6. It is clear that between the points marked as 1, 2 etc. the angular velocity varies slightly. It is also remarkable that, as the particle in the marked positions shows, the particle does not rotate about an axis through its own center.

We are, of course, interested whether Eqs. (5a)–(5b) are able to reproduce the observed orbits and the absence of spinning motion. The resulting range of the Reynolds number is 1400–1500. In this *Re* regime, the expression of Eqs. (3c) and (3d) can be reduced to $g(Re) \approx -2.0$, $C_{W0}(L^*) \propto L^{-2}$. Thus, the wall repulsive force may be written as

$$F_W = \chi L^{-4} A_p \rho u^2/2, \tag{7}$$

where χ is a parameter meant to fit the experimental values to the numerically obtained ones.During orbital motion, the velocity is almost constant, since the fluctuation is about 8% of the average. The latter is in the regime $1400 < Re < 1500$, where the $a(Re)$ changes very little (see Eq. (3c)). So we are justified to take a constant value for χ.A good fit appears to be made with $\chi = 5 \times 10^{-4}$. We used Eq. (5a) and expression (7) for the wall force F_W. We start with analyzing the trajectories. We denote the radius vector of the orbit center, measured from the center of the drum, with $\boldsymbol{r_e}$ and of the momentary position of the sphere with $\boldsymbol{r}$ as shown in Fig. 7 . The particle turns around $\boldsymbol{r_e}$ with instantaneous angular velocity $\boldsymbol{\Omega_p}$ which varies along the orbit. So its velocity is

$$\boldsymbol{u} = \boldsymbol{\Omega_p} x (\boldsymbol{r} - \boldsymbol{r_e}). \tag{8}$$

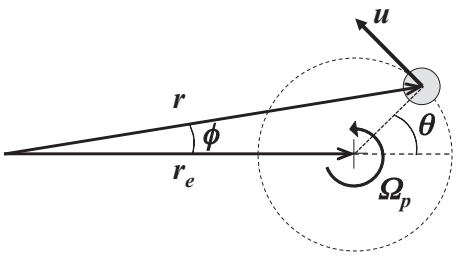

FIG. 7. The equilibrium radius vector $\boldsymbol{r_e}$, the momentary position of the sphere $\boldsymbol{r}$, and the particle velocity $\boldsymbol{u}$. The particle turns around $\boldsymbol{r_e}$ with momentary angular velocity $\boldsymbol{\Omega_p}$. The dashed black line represents the particle circular orbit. The cross marker shows the equilibrium point.

This is the velocity as measured in the laboratory frame. The velocity relative to the surrounding fluid which rotates about the center of the drum with angular velocity, $\boldsymbol{\omega}$, is

$$\boldsymbol{u} - \boldsymbol{\omega}\times\boldsymbol{r} = (\boldsymbol{\Omega_p} - \boldsymbol{\omega})\times(\boldsymbol{r} - \boldsymbol{r_e}) - \boldsymbol{\omega}\times\boldsymbol{r_e}. \tag{9}$$

We have seen that $\boldsymbol{r_e}= (r_e,\phi_e{=}0)$. Hence the velocity $-\boldsymbol{\omega}\times\boldsymbol{r_e}$ for each orbit is directed along the negative y-axis in Fig. 5. We can make an estimate for this from the measurements of the orbits and the velocities. We take the case with the following data: $R = 7\times10^{-3}$ m; $f_d = 0.11$ Hz. The orbit is displayed in Fig. 5 and the velocity relative to the rotating frame in Fig. 10.

We write Eq. (9) as

$$\boldsymbol{u} = -\omega r_e \boldsymbol{e_y} + \Delta\Omega\sigma\boldsymbol{e_\theta} = \langle\boldsymbol{u}\rangle + \boldsymbol{u}', \tag{10}$$

where $\Delta\Omega = |\boldsymbol{\Omega_p} - \boldsymbol{\omega}|$ and $\sigma = |\boldsymbol{r} - \boldsymbol{r_e}|$.

From Fig. 9 we obtain $r_e = 0.15$ m and hence $\langle u\rangle$ should be

$$\langle u\rangle = 2\pi f_d r_e = 0.104. \tag{11}$$

In Fig. 10 the maximum and minimum velocity are 0.111 m/s and 0.099 m/s, respectively, and hence the average is 0.104 m/s which agrees very well. From the difference of these values and considering only the ground frequency, that is,

$$u' = \Delta\Omega_{max}\sigma\cos(\omega t + \phi), \tag{12}$$

where ϕ is a phase angle, we obtain $u' = 6\times10^{-3}\cos(\omega t + \phi)$. From Eq. (10) it appears that the particle "sees" a constant velocity in the negative y-direction and a small fluctuation on top of that. For the calculation, with the help of Eq. (5) we therefore approximate C_D and C_L with the values based on $\langle u\rangle$ with $\phi_e{=}0$. These are

$$C_D = \frac{8}{3}\frac{gR}{(\omega r_e)^2}\frac{\rho_p - \rho}{\rho}, \tag{13a}$$

$$C_L = \frac{1}{2}(1 + C_A). \tag{13b}$$

With these values for C_D and C_L we calculated the particle trajectories for a number of frequencies in the suspended regime 0.07 Hz $< f_d <$ 0.11 Hz. We used the value of χ to fit the calculated results to the measured ones as explained above. The radial position of the center of the particle orbits r_e and the orbit radius S in experiments are plotted as a function of Reynolds number, Re_e in Fig. 8. Here the Reynolds number Re_e is defined as

$$Re_e = \frac{\omega r_e R}{\nu}. \tag{14}$$

For comparison Fig. 8 also shows the same quantities but now obtained numerically. Figure 8 shows an excellent agreement within experimental error. This agreement becomes also clear when comparing the orbits shown in Fig. 5 with those in Fig. 9. It indicates that the force model described by Eq. (5) including the wall repulsive force model in Eq. (3) properly expresses each force acting on a sphere in this Re_e regime.

Next we turn our attention to the observation that the particle hardly spins around the axis through its center, parallel to the axis of the big cylinder as shown in Fig. 11. One would expect that the particle rotates with the local fluid. We suggest here the following explanation. As we have seen, the relative motion of the particle with respect to the fluid consists of a steady velocity in the negative y-direction in Fig. 9, and small fluctuation, given by Eq. (12), in the direction tangential to the path. This produces surface stress in principle leading to rotation of the particle. However these stresses vary with time. For this the period of the cylinder $1/f_d$ is the scale. For a stress to become effective it takes a certain time, i.e., the relaxation time. This has to do with diffusion of vorticity and is of order d^2/ν, where d is the particle diameter and ν the kinematic viscosity of the liquid. Bagchi *et al.*[16] measured relaxation times for spheres in rotational flows at Reynolds number up to 200 and found values about 4 times this quantity. Their work also shows that the relaxation

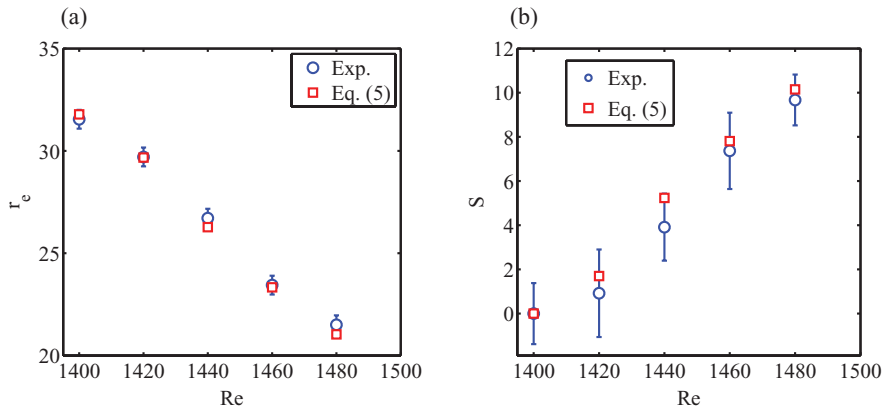

FIG. 8. Comparison between experimental results and numerical solution from Eq. (5) for (a) radial center position and (b) radius of orbital motions as a function of Reynolds number (correspond to the drum frequency 0.07–0.11 Hz).

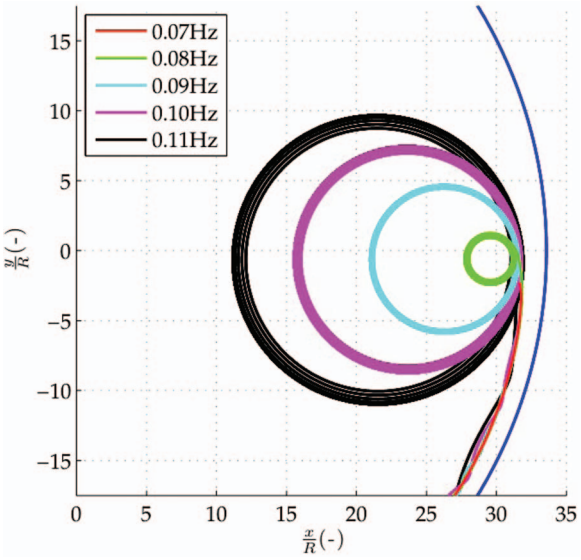

FIG. 9. Paths reproduced by Eq. (5) for the drum frequency 0.07–0.11 Hz.

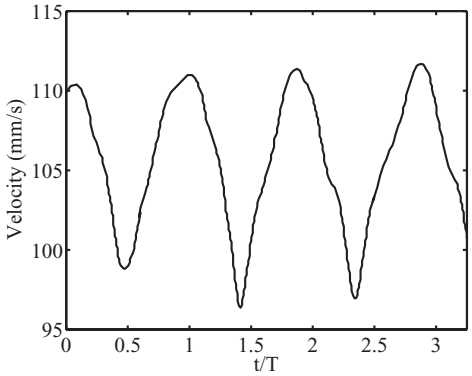

FIG. 10. Magnitude of the particle velocity vs time normalized by the drum time cycle.

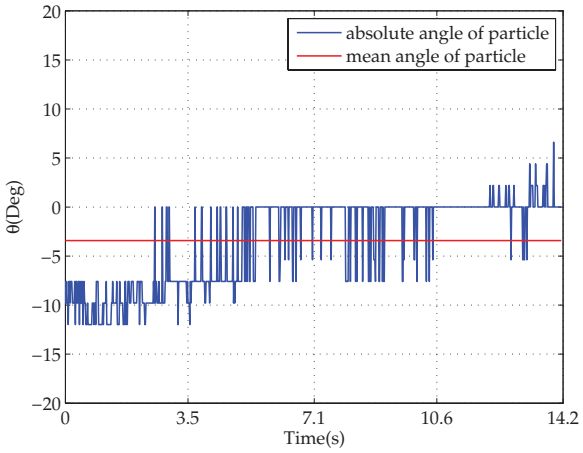

FIG. 11. The absolute angular rotation of the sphere in a solid body rotating flow with $f_d = 0.07$ Hz for one period of the drum.

time increases with increasing Reynolds number. We have Reynolds numbers of order 10^3 and with an estimate of τ as

$$\tau = \frac{2d^2}{\nu} \sim 400, \tag{15}$$

we are on the conservative side. With f_d= 0.11 Hz, τ is much larger than $1/f_d$. This means that an applied stress gets no time to produce a significant rotation. Thus it can only give very little response to the rapidly varying velocity while orbiting.

As described above, the orbits from Eq. (5) with the wall repulsive force model can reproduce the experimental results. This suggests that even though the wall force model (Eq. (3)) by Takemura *et al.*[9] was made for a rising sphere near a vertical planar wall, it seems to be valid for the case of solid-body rotation in the present *Re* regime. In addition, we performed PIV measurements. A snapshot of the flow field is shown in Fig. 12(a). In our analysis an undisturbed velocity towards the particle is assumed. Indeed Fig. 12(b) shows that the upstream flow of the particle at $\psi = -14.5^\circ$ is undisturbed solid body rotation. This is quite different in the case of a cylinder in the rotating flow.[17] Downstream from the particle a wake is clearly visible. This wake is deflected towards the center of the cylinder.

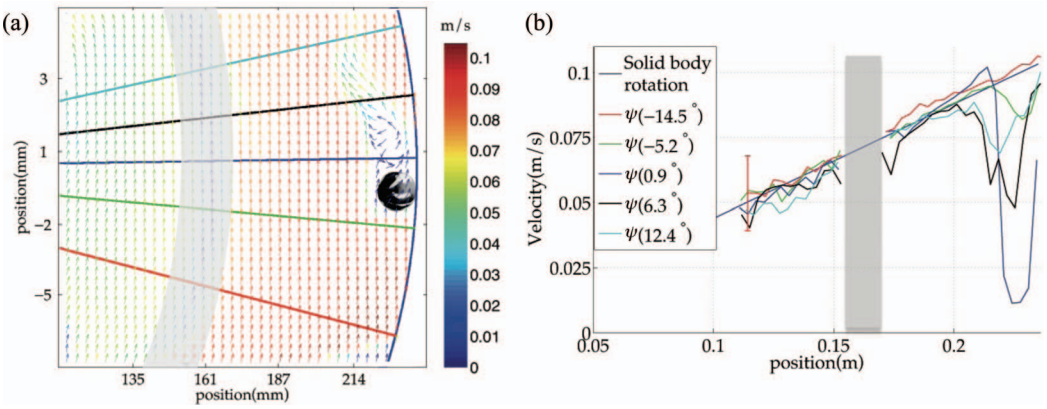

FIG. 12. The result of the flow field around a 7 mm particle in a drum at $f_d = 0.07$ Hz using particle image velocimetry. (a) Flow field and (b) Velocities vs. positions along the lines shown in the left panel.

V. CONCLUSIONS

We study translational and rotational motion of a particle slightly heavier than the fluid in a rotating drum filled with water. Remarkably in the regime of 0.07 Hz $\leq f_{drum} \leq$ 0.11 Hz the particle is found to be suspended in the drum with an orbital motion, which was not observed by Ashmore *et al.*[12] We investigate the force balance by including the effect of the drum wall (F_W) modeled as $F_W \propto L^{-4}$.[9,10] The orbits of the particle from the force balance including F_W nicely reproduce the experimental trajectories. We also investigate the spin of a particle. The particle orientation changes less than 10° over one cycle of the drum due to the small torque acting on the sphere.

ACKNOWLEDGMENTS

We acknowledge support from the EU COST Action MP0806 on "Particles in Turbulence." We thank Devaraj van der Meer and Detlef Lohse for fruitful discussions.

[1] J. Magnaudet and I. Eames, "The motion of high-Reynolds-number bubbles in inhomogeneous flows," Annu. Rev. Fluid Mech. **32**, 659 (2000).
[2] E. A. V. Nierop, S. Luther, J. J. Bluemink, J. Magnaudet, A. Prosperetti, and D. Lohse, "Drag and lift forces on bubbles in a rotating flow," J. Fluid Mech. **571**, 439 (2007).
[3] J. J. Bluemink, E. A. V. Nierop, S. Luther, N. G. Deen, J. Magnaudet, A. Prosperetti, and D. Lohse, "Asymmetry-induced particle drift in a rotating flow," Phys. Fluids **17**, 072106 (2005).
[4] J. J. Bluemink, D. Lohse, A. Prosperetti, and L. van Wijngaarden, "A sphere in a uniformly rotating or shearing flow," J. Fluid Mech. **600**, 1 (2008).
[5] J. J. Bluemink, D. Lohse, A. Prosperetti, and L. van Wijngaarden, "Drag and lift forces on particles in a rotating flow," J. Fluid Mech. **643**, 1 (2010).
[6] M. Rastello, J.-L. Marié, N. Grosjean, and M. Lance, "Drag and lift forces on interface-contaminated bubbles spinning in a rotating flow," J. Fluid Mech. **624**, 159 (2009).
[7] M. Rastello, J.-L. Marié, and M. Lance, "Drag and lift forces on clean spherical and ellipsoidal bubbles in a solid-body rotating flow," J. Fluid Mech. **682**, 434 (2011).
[8] G. O. Roberts, D. Kornfeld, and W. Fowlis, "Particle orbits in a rotating liquid," J. Fluid Mech. **229**, 555–567 (1991).
[9] F. Takemura and J. Magnaudet, "The transverse force on clean and contaminated bubbles rising near a vertical wall at moderate Reynolds number," J. Fluid Mech. **495**, 235–253 (2003).
[10] L. Zeng, S. Balachandar, and P. Fischer, "Wall-induced forces on a rigid sphere at finite Reynolds number," J. Fluid Mech. **536**, 1 (2005).
[11] Q. Liu and A. Prosperetti, "Wall effects on a rotating sphere," J. Fluid Mech. **657**, 1 (2010).
[12] J. Ashmore, C. D. Pino, and T. Mullin, "Cavitation in a lubrication flow between a moving sphere and a boundary," Phys. Rev. Lett. **94**, 124501 (2005).
[13] T. Mullin, Y. Li, C. D. Pino, and J. Ashmore, "An experimental study of fixed points and chaos in the motion of spheres in a Stokes flow," IMA J. Math. Appl. Med. Biol. **70**, 666 (2005).
[14] R. Zimmermann, Y. Gasteuil, M. Bourgoin, R. Volk, A. Pumir, and J.-F. Pinton, "Rotational intermittency and turbulence induced lift experienced by large particles in a turbulent flow," Phys. Rev. Lett. **106**, 154501 (2011).
[15] I. Mazzitelli, D. Lohse, and F. Toschi, "On the relevance of the lift force in bubbly turbulence," J. Fluid Mech. **488**, 283 (2003).
[16] P. Bagchi and S. Balachandar, "Effect of free rotation on the motion of a solid sphere in linear shear flow at moderate Re," Phys. Fluids **14**, 2719 (2002).
[17] C. Sun, T. Mullin, L. van Wijngaarden, and D. Lohse, "Drag and lift forces on a counter-rotating cylinder in rotating flow," J. Fluid Mech. **664**, 150 (2010).